THE JOURNAL OF BIOLOGICAL CHEMISTRY VOL. 282, NO. 18, pp. 13917–13927, May 4, 2007

The Immunoglobulin Heavy Chain Constant Region Affects Kinetic and Thermodynamic Parameters of Antibody Variable Region Interactions with Antigen*[S]

Received for publication, January 23, 2007, and in revised form, March 2, 2007 Published, JBC Papers in Press, March 12, 2007, DOI 10.1074/jbc.M700661200

Marcela Torres[‡], Narcis Fernández-Fuentes[§], András Fiser[§], and Arturo Casadevall[‡1]

From the Departments of [‡]Microbiology & Immunology and [§]Biochemistry, Albert Einstein College of Medicine, Bronx, New York 10461

A central dogma in immunology is that antibody specificity is a function of the variable (V) region. However serological analysis of IgG_1, IgG_{2a}, and IgG_{2b} switch variants of murine monoclonal antibody (mAb) 3E5 IgG_3 with identical V domains revealed apparent specificity differences for *Cryptococcus neoformans* glucuronoxylomannan (GXM). Kinetic and thermodynamic binding properties of mAbs 3E5 to a 12-mer peptide mimetic of GXM revealed differences in the affinity of these mAbs for a monovalent ligand, a result that implied that the constant (C) region affects the secondary structure of the antigen binding site, thus accounting for variations in specificity. Structural models of mAbs 3E5 suggested that isotype-related differences in binding resulted from amino acid sequence polymorphisms in the C region. This study implies that isotype switching is another mechanism for generating diversity in antigen binding and that isotype restriction of certain antibody responses may reflect structural constraints imposed by C region on V region binding. Furthermore, isotype affected the polyreactivity of V region identical antibodies, implying a role for C region in determining self-reactivity.

Antibodies are heterodimeric proteins composed of two heavy (H)[2] and two light (L) chains. Each H and L chain contains a V domain that when combined defines the antigen (Ag) binding site. In the mammalian genome, there are five major classes of heavy constant (C_H) domains that determine Ab isotype. These are usually assumed to have effector functions without directly affecting the Ag binding affinity and/or specificity. However, the C_H domains are known to contribute to the apparent affinity through avidity effects that result from the polyvalent nature of certain immunoglobulins (Ig) classes. Hence, the classical view of Ig function is that the V domains are solely responsible for Ab affinity and specificity, whereas the C region is responsible for the biological properties such as complement activation, Fc receptor binding, avidity, and serum half-life (1). This concept posits that when B cells switch from one C_H region to another, the avidity and effector functions of an Ab change without altering the specificity for the antigen (2). However, V region-identical Abs have been reported to manifest differences in the magnitude of binding to Ag, fine specificity, and idiotypic (Id) recognition (3–7), thus challenging this central immunological dogma.

A critical condition for Ab-Ag binding is the formation of a specific complex between the Ab and the Ag. Understanding the interaction of these two biological macromolecules requires detailed knowledge of the structure and functional characteristics of the complex. The structure of the Ab-Ag complex can be described using x-ray crystallography and computer-generated structural models. The functional activity can be described by the kinetic rate constants ($k_{on/off}$), equilibrium constants (K), and thermodynamic parameters of the binding complex. The equilibrium constant is related to the Gibbs free energy of binding (ΔG) by the relationship $\Delta G = -RT\ln K_A = \Delta H - T\Delta S$. A net negative change in ΔG indicates successful binding interactions, and the magnitude of this change directly determines the binding affinity. ΔG involves and is modulated by two other thermodynamic parameters, the enthalpy change (ΔH) and the entropy change (ΔS) (8, 9). Enthalpy describes heat changes resulting from molecular interactions at the binding site involving electrostatic, hydrophobic, hydrogen bonds, and van der Waals intermolecular interactions, whereas entropy changes reflect the net conformational, stereochemical, and structural perturbations that occur within the interacting entities or in the surrounding solvent molecules (8, 9).

Our previous studies using a family of mouse-human chimeric (ch) Abs and two families of murine IgG isotype switches demonstrated that isotype contributes to Ab fine specificity differences for multivalent Ags by showing differences in binding and Id recognition for these mAbs to their Ags (7, 10). Those studies relied entirely on serological methods to investigate binding differences. To formally prove the notion that the C_H region affects binding to a monovalent ligand, we have used surface plasmon resonance (SPR) in a Biacore system. SPR allows measurements of the formation and dissociation of com-

* This work was supported by Grants AI33774, AI33142, and HL59842 from the National Institutes of Health. The costs of publication of this article were defrayed in part by the payment of page charges. This article must therefore be hereby marked "*advertisement*" in accordance with 18 U.S.C. Section 1734 solely to indicate this fact.

[S] The on-line version of this article (available at http://www.jbc.org) contains supplemental Figs. 1S–3S and Tables 1S and 2S.

[1] To whom correspondence should be addressed: Dept. of Microbiology and Immunology, Albert Einstein College of Medicine, 1300 Morris Park Ave., Forchheimer Bldg., Rm. 411, Bronx, NY 10461. Tel.: 7180-430-2811; Fax: 7180-430-8701; E-mail: casadeva@aecom.yu.edu.

[2] The abbreviations used are: H, heavy chain; L, light chain; GXM, glucuronoxylomannan; Ab, antibody; mAb, monoclonal antibody; Ag, antigen; C, constant region; V, variable region; ch, chimeric; SPR, surface plasmon resonance; Fab, antigen-binding fragment; Id, idiotype/idiotypic; K, equilibrium constant; k, kinetic rate constant; ΔG, Gibbs free energy; ΔH, enthalpy; ΔS, entropy; BSA, bovine serum albumin; PBS, phosphate-buffered saline; TBS, Tris-buffered saline; MES, 2-(*N*-morpholino)ethanesulfonic acid.

plexes, in real time and in a label-free environment. Using SPR analysis we determined the kinetic and thermodynamic constants for the interaction of V region-identical IgG_1, IgG_{2a}, IgG_{2b}, and IgG_3 with a monovalent Ag in the form of peptide mimetic. The binding kinetics are best described by a two-state bimolecular association model consistent with an Ab and Ag encounter step followed by a docking step, which may include conformational rearrangements. Consequently, the results presented here indicate kinetic and thermodynamic variations that imply diverse Ab-Ag interactions within IgG molecules expressing different C_H regions but identical V regions.

EXPERIMENTAL PROCEDURES

mAbs and Peptides—GXM-binding mAb 3E5 (IgG_3) was produced by a hybridoma isolated from a mouse immunized with a GXM-tetanus toxoid conjugate vaccine (11). The IgG_1, IgG_{2a}, and IgG_{2b} switch variants of 3E5 IgG_3 were generated *in vitro* by sib selection (12). Members of the mAb 3E5 family share identical V_H and V_L sequences (7). All murinem mAbs were purified by protein A or G affinity chromatography (Pierce) from hybridoma culture supernatants and dialyzed against PBS. mAb concentration was determined by ELISA and Bradford measurements. All Abs were tested by PAGE to verify their integrity and correct molecular weight. mAbs 3E5 were analyzed by MALDI-TOF (matrix-assisted laser desorption ionization time-of-flight) mass spectrometry at the Laboratory for Macromolecular Analysis, Albert Einstein College of Medicine, to confirm the absence of mAb aggregates (7, 13). Peptide mimetic P1 (SPNQHTPPWMLK) (7) was synthesized and biotinylated by the Laboratory for Macromolecular Analysis, Albert Einstein College of Medicine.

Generation of Fabs—Fabs were generated from mAbs 3E5 IgG_{2a} and 3E5 IgG_3. mAb 3E5 IgG_{2a} was dialyzed against 20 mM Na_2PO_4, 10 mM EDTA, pH 7.0, before enzymatic digestion. Papain digestion was carried out overnight at room temperature in 20 mM Na_2PO_4, 10 mM EDTA, pH 7.0, and 0.8 mM dithiothreitol with an *E*:S ratio of 1:20. mAb 3E5 IgG_3 was dialyzed against 20 mM Tris-NaCl pH 7.4, before enzymatic digestion. Papain digestion was carried out overnight at room temperature in 20 mM Tris-NaCl, pH 7.4, and 0.8 mM dithiothreitol with an *E*:S ratio of 1:20. After digestion, Fab molecules from both mAbs were purified by protein A affinity chromatography (Pierce) and dialyzed against at least two changes of PBS.

GXM-3E5 mAbs Binding ELISA at Different pHs—Polystyrene plates were coated with a 5 μg/ml solution of GXM in PBS, incubated 1.5 h at 37 °C, and blocked overnight at 4 °C with 1% BSA in TBS. mAbs 3E5 were added at 50 μg/ml in 0.2 M phosphate buffer at pH ranging from 4.4 to 10.4 and serially diluted. The plates were incubated for 1.5 h at 37 °C. mAb binding was determined with alkaline-phosphatase-conjugated goat anti-mouse κ (Southern Biotech) and *p*-nitrophenyl phosphate substrate by measuring absorbance at 405 nm.

GXM-3E5 mAbs Binding ELISA in Ethanol—Polystyrene plates were coated with a 5 μg/ml solution of GXM in PBS, incubated 1.5 h at 37 °C, and blocked with 1% BSA in TBS. mAb was added at 50 μg/ml in 5% ethanol, 1% BSA. Serial dilutions were made, and plates were incubated for 1.5 h at 37 °C. mAb binding was determined as above.

Polyreactivity ELISA—mAbs 3E5 were screened for polyreactivity against a panel of antigens by ELISA. Polystyrene plates were coated overnight at 4 °C with actin (Sigma), tubulin (ICN), and thyroglobulin (Sigma) at 5 μg/ml in bicarbonate buffer, pH 9.6, and with double-stranded DNA (Sigma) and single-stranded DNA (Sigma) at 100 μg/ml in sodium citrate buffer, pH 6.0. Plates were blocked with 1% BSA in TBS for 2 h at 4 °C. mAbs were added at 50 μg/ml in 1% BSA/TBS and serially diluted. Plates were incubated overnight at 4 °C. mAb binding was determined with alkaline-phosphatase-conjugated goat anti-mouse κ (Southern Biotech) and *p*-nitrophenyl phosphate substrate by measuring absorbance at 405 nm.

Immobilization of 3E5 mAbs onto CM5 Chips—The Biacore 3000 system and research grade sensor chip CM5 (Biacore) were used. mAbs and Fabs were immobilized on the surface of a CM5 chip through primary amino groups using reactive esters. The carboxylated matrix was first activated with 70 μl of a 1:1 mixture of *N*-ethyl-*N*′(dimethylaminoporpyl)-carbodiimide (Pierce) and *N*-hydroxysuccinimide (Pierce). mAbs 3E5 were injected at 25 μg/ml in 10 mM MES (Sigma-Aldrich), pH 6.0. Fab 3E5 IgG_{2a} and Fab 3E5 IgG_3 were injected at 100 and 50 μg/ml, respectively, in 10 mM sodium acetate (Sigma-Aldrich), pH 4.99. After mAb injection, remaining *N*-hydroxysuccinimide ester groups were blocked by an injection of 70 μl of 1 M ethanolamine (Sigma-Aldrich), pH 8.5.

Biacore Binding Assays—Peptide mimetic of GXM P1 was used to analyze the kinetic and thermodynamic parameters of the mAbs utilized in this study. This peptide was recovered from a peptide phage display library screened with 3E5 IgG_3, and it has been previously shown to bind all mAb 3E5 isotypes (7). The interaction of the mAb-peptide complexes was analyzed at 10, 15, 20, 25, 30, and 35 °C. Peptide P1 was tested at concentrations ranging from 1.56 to 200 μM at high flow rate (100 μl/min) in 0.2 mM K_2HPO_4/KH_2PO_4, pH 6.5, 150 mM KCl, and 0.05% P20. At the end of the dissociation phase, the surface was regenerated by injecting 50 μl of 50 mM ethanolamine in 50% ethylene glycol (Sigma-Aldrich) and 50 μl of 10 mM HCl. Nonderivatized flow cells served as a reference surface. The continuous flow ensured that no changes in analyte concentration occurred during the measurements. The availability of a constant free analyte concentration is particularly important for the determination of kinetic parameters. By using one of the flow channels as an in-line reference, a control is obtained on the same sample aliquot, eliminating the variations that occur with separate reference and sample measurements. Kinetic data were interpreted with BIAevaluation 4.1 software. Data for each group were analyzed globally using a two-state model to obtain the individual forward (k_{+1}, k_{+2}) and reverse (k_{-1}, k_{-2}) rate constants. The rate constants for each global fit were used to calculate the equilibrium constant (K_A).

$$K_{a1} = k_1/k_{-1} \quad \text{(Eq. 1)}$$

$$K_{a2} = k_2/k_{-2} \quad \text{(Eq. 2)}$$

$$K_A = K_{a1}(1 + K_{a2}) \quad \text{(Eq. 3)}$$

The Gibbs free energy changes (ΔG) were calculated from the equilibrium constants,

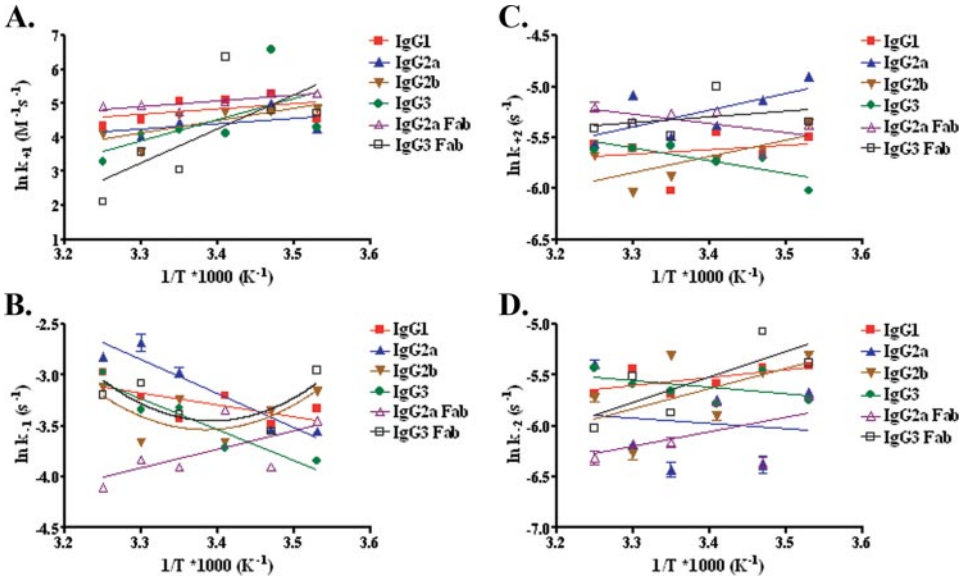

FIGURE 1. **Analysis of the association and dissociation rates constants by SPR.** Van't Hoff plots of the rate constants k_{+1} (*A*), k_{-1} (*B*), k_{+2} (*C*), and k_{-2} (*D*) for mAbs 3E5 binding to peptide P1. All data points were obtained from the BIAevaluation 4.1 software using a two-state model. *Lines* represent the best fit to a linear regression using a 95% confidence interval. *Errors bars* were calculated using propagation of error for S.E. of each assay.

$$\Delta G_1 = -RT\ln K_{a1} \quad \text{(Eq. 4)}$$

$$\Delta G_2 = -RT\ln K_{a2} \quad \text{(Eq. 5)}$$

$$\Delta G = -RT\ln K_A = \Delta G_1 + \Delta G_2 \quad \text{(Eq. 6)}$$

$$\Delta G = \Delta H - T\Delta S \quad \text{(Eq. 7)}$$

By rearranging the equations above, we can rewrite the relationship into

$$\ln K_A = -\Delta H/RT + \Delta S/R \quad \text{(Eq. 8)}$$

By measuring K_A as a function of temperature, one can draw a plot of $\ln K_D$ ($1/K_A$) *versus* $1/T$. Ideally, this plot, known as a van't Hoff plot, should yield a straight line with a slope of $-\Delta H/R$ and an intercept $\Delta S/R$. Enthalpy changes (ΔH) were calculated from the slope of the van't Hoff plot. Entropy changes (ΔS) were calculated from the equation $\Delta G = \Delta H - T\Delta S$ by substituting the values of ΔG (from $\Delta G = -RT\ln K_A$) and assuming ΔH is constant with temperature. Equilibrium affinity constants were calculated without considering the errors of the rate constants.

Molecular Modeling—The variable domains of the heavy and light chains of mAbs 3E5 IgG_1, IgG_{2a}, IgG_{2b}, and IgG_3 sequences are identical. Thus, only one set of sequences corresponding to the V_H and V_L sequences of 3E5 IgG_1, with accession numbers AAT81538 and AAT81540, were downloaded from GenBank™ (14). Each sequence was used to scan the Protein Data Bank (15) using PSI-BLAST (16) with default parameters. PSI-BLAST outputs were filtered using BlastProfiler (17) to select templates with the highest sequence coverage and high sequence identity. Selected templates were inspected manually to choose those with the highest crystallographic quality. The models were built with MODELLER (18, 19), combining two experimental structures as templates for each sequence. A common structure for all sequences (Protein Data Bank code 2h1p), was used as template for V and C regions of both the L and H chains and a specific template for the C_{H1} domain depending on the Ab isotype (Protein Data Bank codes 1sbs, 1jgu, 2cgr, and 1pz5 for IgG_1, IgG_{2a}, IgG_{3b}, and IgG_3 C_{H1} domain, respectively). The 2h1p structure corresponds to the experimental three-dimensional structure of anti-GXM mAb 2H1 with peptide mimetic of GXM PA1. The average sequence identity between target sequences and templates was greater than 90%, assuring high quality models (19). Five models were generated for each mAb, and the one with lowest energy (according to MODELLER energy function) was selected and further analyzed with PROSA-II (20) and PROCHECK (21) to determine the quality of the models.

Identifying "Highly Connected" Regions—Structural models were submitted to the SARIG (structural analysis of residue interaction graphs) server (22). The SARIG server converts protein structures into residue interaction graphs (RIGs) in which amino acid residues serve as the nodes of the graph and their interatomic contacts with each other are the graph edges. SARIG analyzes the so-called closeness of the residue(s). Closeness is a property that measures how close each node (or residue) is to all other nodes in the network. The distance is defined as the length of the shortest path between the two nodes. Closeness values are expressed in Zscores and thus are standardized by the standard deviation from the mean value calculated for each protein structure. It was shown that functionally important residues typically have high closeness values. Residues with high closeness values, *i.e.* highly connected ones, may interact directly or through intermediates (allostery) with other residues of the protein.

RESULTS

One-step Versus Two-step Kinetic Models—We chose the two-state model based on the proposal that these mAbs may have changes in their Fab structure or Ig surface properties, which could be a result of binding to Ag (7). The two-step model fitted better than one-step model to our experimental data (Fig. 1S in supplemental data, and data not shown) and it has been shown to be a more precise representation of Ab-Ag interactions (23, 24). The simulated curves generated with the two-state model were almost identical to the experimental curves (data not shown). In addition, we found that the Langmuir one-step binding model was not applicable because of the higher apparent affinity obtained with intact IgG. Thus, binding kinetics indicates that mAbs 3E5-P1 complexes are best described by a two-state model,

$$A + B \underset{k_{-1}}{\overset{k_{+1}}{\rightleftharpoons}} AB^* \underset{k_{-2}}{\overset{k_{+2}}{\rightleftharpoons}} AB$$

REACTION 1

This model allows the estimation of two forward rates constants (k_{+1}, k_{+2}) and two reverse rate constants (k_{-1}, k_{-2}). The rate constants k_{+2} and k_{-2} are not true on- and off-rate constants but rather are the rates of monomolecular complex conversion between the docked and undocked form. The rate constants k_{+2} and k_{-2} modulate the observed on- and off-rates when they become rate-limiting, *i.e.* when $k_{+2} < k_{+1}$ or $k_{-2} < k_{-1}$ (25). The fitting of sensorgram data to a two-state model (supplemental data, Fig. 1S) is significantly better than to a one-step model based on low and evenly distributed residuals, low χ^2 (<1), and visual inspection of the binding curves. This fitting is not attributable to heterogeneity of the IgG sample or to nonspecific interactions, because all mAbs were obtained from hybridoma culture supernatant, affinity-purified, and tested for GXM binding by ELISA. PAGE and mass spectrophotometry were used to verify mAb integrity and to discard the possibility that some of our results were due to the presence of mAb aggregates.

Effect of Antibody Subclass on the Kinetic and Equilibrium Rate Constants—SPR analysis revealed differences between the binding kinetics of the mAbs 3E5-P1 complexes that were also observed throughout the temperature range studied. Examination of the dissociation equilibrium constants and individual rate constants indicates that all four Abs and the two Fabs exhibited different kinetic and thermodynamic properties on binding. These changes were also observed with variation in temperature. Furthermore, the magnitude of the temperature effect was characteristic for each Ab-peptide complex (Figs. 1 and 2). Rate and equilibrium constants also revealed that the variation in temperature had different impacts on the encounter and docking steps.

Slightly different results were observed for the effect of temperature on the association and dissociation rates of mAb 3E5-P1 complex formation with the different isotypes. For all complexes, the encounter forward rate constant (k_{+1}) decreased at higher temperatures (Fig. 2*A*). Fig. 1*C* shows that for 3E5 IgG_1-P1, IgG2a-P1, and IgG_{2b}-P1 complexes, the docking association rate constant (k_{+2}) decreased at high temperatures, whereas for 3E5 IgG_3, Fab IgG_{2a}, and Fab IgG_3 the magnitude of this parameter increased. The curves for the encounter reverse rate constant (k_{-1}) increased at higher temperatures for 3E5 IgG_1-P1, IgG_{2a}-P1, and IgG_3-P1 complexes, whereas for Fab 3E5 IgG_{2a}-P1 complex a decrease of k_{-1} was observed. For 3E5 IgG2b-P1 and Fab 3E5 IgG_3-P1 complexes, the data most closely fit a curvilinear regression, and therefore these interactions appeared to be more complex (Fig. 1*B*). The plots for docking reverse rate constant (k_{-2}) showed a decrease with a temperature increase for 3E5 IgG_{2a}-P1, IgG_{2b}-P1, and Fab IgG_3-P1 complexes, whereas k_{-2} increased with temperature for the remaining complexes (Fig. 1*D*). However, quantitatively the individual rate constants showed differential response to temperature, with variations on the amount of these decreases between mAbs 3E5-P1 complexes.

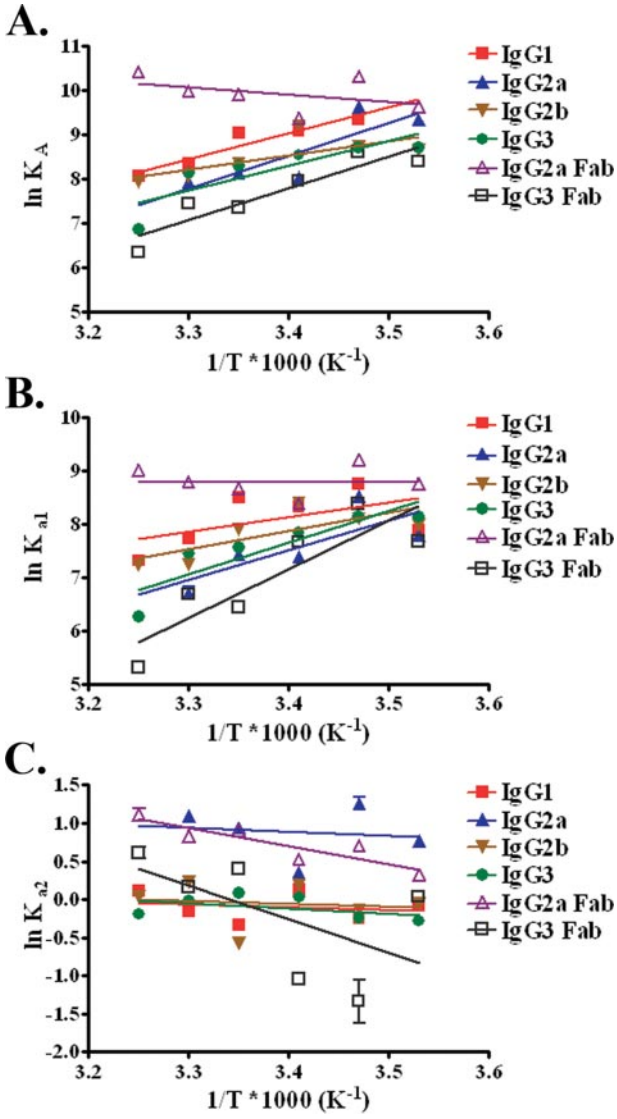

FIGURE 2. **Equilibrium affinities for the binding of mAbs 3E5 to peptide P1.** Van't Hoff plots of the equilibrium association rate constant (K_A) (*A*), encounter equilibrium association rate constant (K_{a1}) (*B*), and docking equilibrium association rate constant (K_{a2}) (*C*) for mAbs 3E5 binding to peptide P1. All equilibrium constants were calculated from the rate constant obtained from the fittings to a two-state model. *Lines* represent the best fit to a linear regression using a 95% confidence interval. *Errors bars* were calculated using propagation of error for S.E. of each assay.

The differences in the rate constants for these complexes accounted for the variations observed in the equilibrium rate constants. The affinity of mAbs 3E5 for peptide P1 calculated from the van't Hoff plots decreased at higher temperatures, except for Fab 3E5 IgG_{2a}, in which affinity for the peptide increased (Fig. 2*A*). The equilibrium constants for the encounter steps (K_{a1}) for these complexes decreased as temperature increased, except for the 3E5 Fab IgG_{2a}-P1 complex, where K_{a1} increased (Fig. 2*B*). For the IgG_{2a}-P1 complex, the decrease of k_{-1} (Fig. 1*C*) as a function of temperature may contribute to the temperature increase of K_{a1}. Also, it is noticeable that the van't Hoff plots for the encounter association constant K_{a1} were approximately parallel to those for the overall affinity constants K_A (Fig. 2*A*). In contrast, the docking equilibrium constants (K_{a2}) were relatively insensitive to changes in temperature for

all complexes (Fig. 2*C*), with the exception of the Fab 3E5 IgG_{2a}-P1 complex where this parameter decreased at lower temperatures. The K_{a2} of the Fab 3E5 IgG_3 also decreased initially at lower temperatures but increased again at temperatures below 15 °C (288 K) (Fig. 2*C*). The decrease of overall affinity with increasing temperatures reflects a primary temperature-related reduction in the encounter equilibrium constants of the mAbs 3E5-P1 complexes except for the Fab 3E5 IgG_{2a}-P1 complex. For this complex, the increase in overall affinity reflects a temperature-related increase in the encounter equilibrium constant.

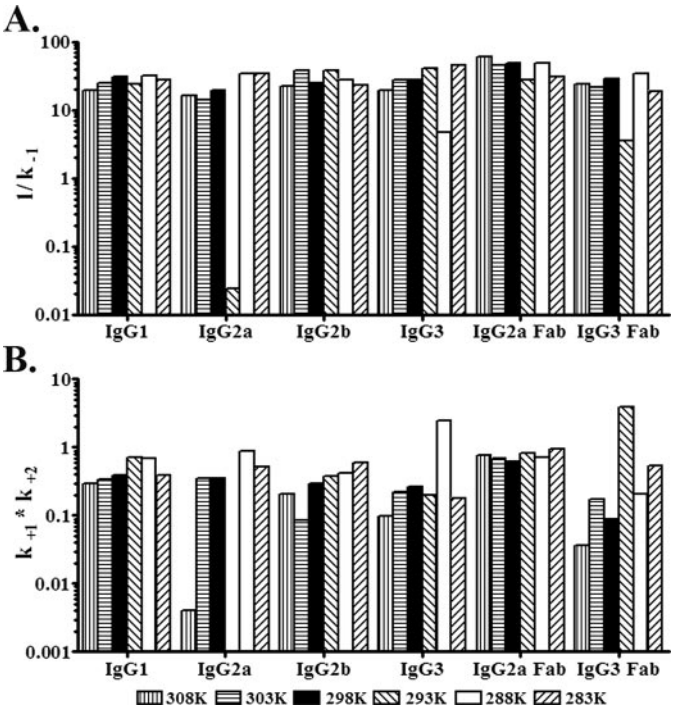

FIGURE 3. **Effect of temperature on the stability and steering of mAbs 3E5 for the binding to peptide P1.** The tendency of the encounter complex to evolve into the final docked complex is proportional to $k_{+1}k_{+2}/k_{-1}$, where $1/k_{-1}$ relates to the stabilization of the docked complex (*A*) and $k_{+1}{}^{*}k_{+2}$ relates to the contribution of electrostatic forces to molecular steering (*B*). Each *bar* represents a different temperature value in degrees Kelvin.

The k_{+2}/k_{-1} ratio is a sensitive indicator of favorable docking (23, 26). Throughout the range of temperatures studied, this ratio is <1 (supplemental data, Table 2S) suggesting that all mAb 3E5-P1 complexes are more likely to remain at the encounter step than to dock. In addition, $k_{+1} > k_{+2}$ for all mAbs 3E5 binding to P1 at the entire range of temperature, thus increasing the time required for the complexes to reach equilibrium and making the docking step rate-limiting. Because of the slower docking and faster dissociation of the encounter complex, the apparent association rate constant for the mAbs 3E5-P1 interactions appeared to be much slower than it is. The reaction rates can be modified through the action of long range electrostatic forces, which can maneuver a protein complex into a different configuration, a phenomenon known as electrostatic steering (27, 28). The stability of the encounter complex is proportional to $1/k_{-1}$ (Fig. 3*A*), whereas the relative overall impact on electrostatic steering from the changes in rate constants due to the associated C_H regions is related to the product of $k_{+1}k_{+2}$ (Fig. 3*B*). The overall stability for mAbs 3E5-P1 complexes are similar (Fig. 3*A*), thus suggesting that the proportion of the complexes within the steering region is comparable for each isotype. In addition, there is an overall increase in the electrostatic steering of Fab 3E5 IgG_{2a} relative to the intact molecule (Fig. 3*B*), and thus this complex will form an encounter complex faster. In contrast, there was an overall decrease in the electrostatic steering for the Fab 3E5 IgG_3 relative to the parental mAb (Fig. 3*B*), and thus this complex will form an encounter complex more slowly than 3E5 IgG_3.

Antibody Subclass Has Different Effects on the Thermodynamic Parameters—The variation in the relative responses reflects differences in the encounter and docking rate constants for the different mAb 3E5-P1 complexes. ΔG decreases with temperature for Fab 3E5 IgG_{2a}-P1 complex while increasing for the remaining complexes (Fig. 4*A*). When the encounter and docking energies of binding, ΔG_1 and ΔG_2, respectively, are considered individually, a similar trend of ΔG_1 (Fig. 4*B*) with respect to ΔG is noticeable (Fig. 4*A*). In contrast, the binding energies of docking (ΔG_2) are relative constant throughout the temperature range examined (Fig. 4*C*), with a slight decrease at high temperatures for Fab 3E5 IgG_{2a}-P1 and Fab 3E5 IgG_3-P1 complexes. From these data, we can establish that for all of these interactions most of the free energy changes come from the encounter step (ΔG_1). Also, the differences in ΔG ($\Delta\Delta G$) for the mAbs 3E5-P1 interactions with respect to

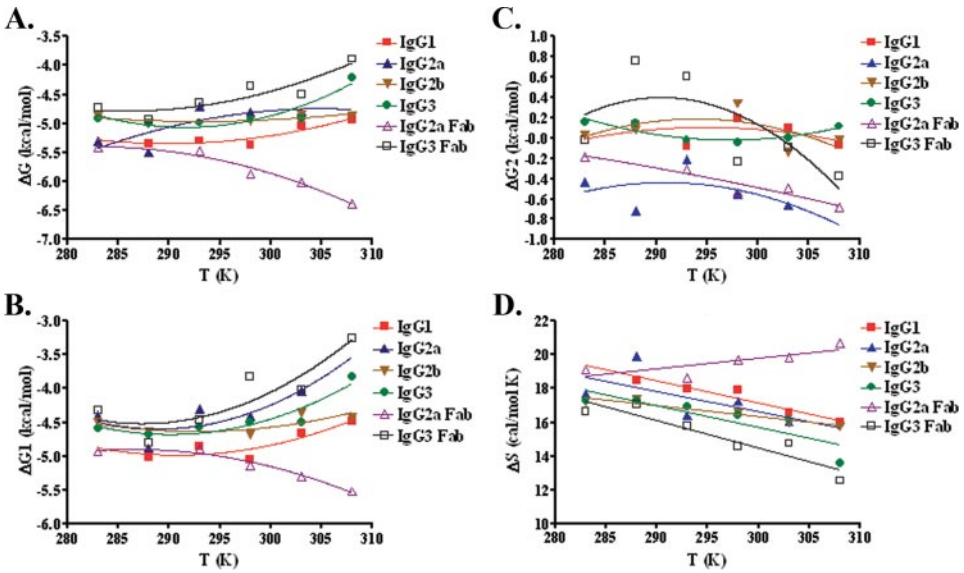

FIGURE 4. **Thermodynamics of binding of mAbs 3E5 to a peptide mimetic of GXM.** Behavior of free energy of binding (ΔG) (*A*), encounter free energy of binding (ΔG_1) (*B*), docking free energy of binding (ΔG_2) (*C*), and entropy of binding (ΔS) (*D*) as a function of temperature for the mAb 3E5 binding to peptide P1. Free energies were calculated from the formula $\Delta G = -RT\ln K_A$, $\Delta G = -RT\ln K_{a1}$, $\Delta G = -RT\ln K_{a2}$, and ΔS is from the formula $\Delta G = \Delta H - T\Delta S$.

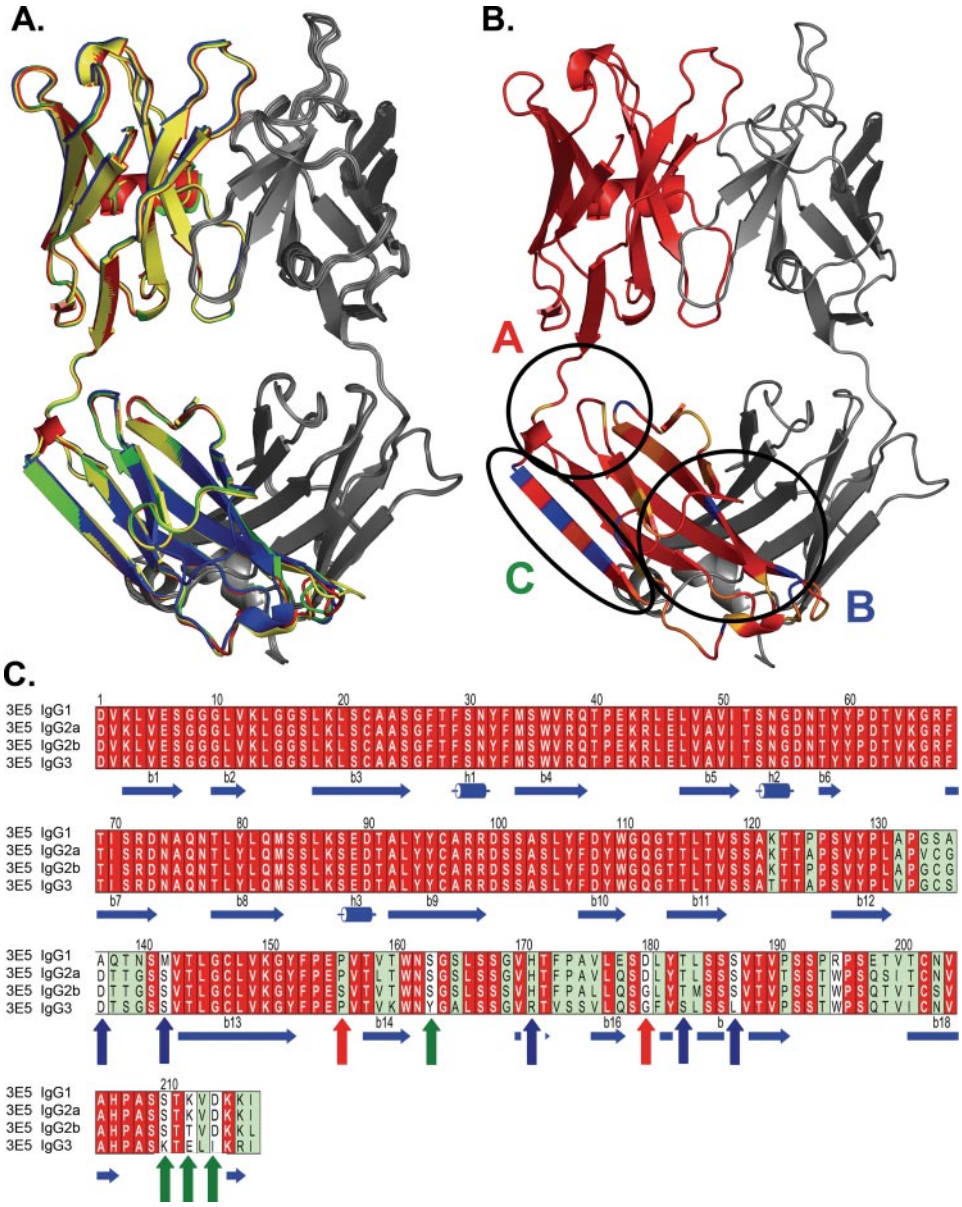

FIGURE 5. **Homology models and the corresponding sequences of 3E5 mAbs V-C_{H1} domains.** *A*, structural superimposition of mAbs 3E5 V_H-C_{H1} is shown in *color*, whereas the associated light chain is *gray*. *B*, homology-based model of 3E5 IgG switch variants shows three regions of structural differences within the C_{H1} domain (regions A, B, and C are indicated by *circles*). *C*, amino acid sequences for the V_H-C_{H1} region of the 3E5 IgG switch variants; *arrows* indicate structural differences in their amino acid sequences (*red*, *blue*, and *green arrows* for regions A, B, and C, respectively). This figure was generated using PyMOL.

the parental 3E5 IgG_3 increased with higher temperatures (supplemental data, Fig. 2S). Furthermore, if we compare the difference of energy of the encounter and docking steps of 3E5 IgG_{2a} with the parental 3E5 IgG_3, there is an overall increase in the binding energies at all temperatures for the docking step ($\Delta\Delta G_2 < -0.5$ kcal/mol) (supplemental data, Fig. 2S), indicating that the associated C_H region of an Ab can affect the energy of binding. This favoring in energy includes its Fab counterpart, Fab 3E5 IgG_{2a}, in which both $\Delta\Delta G_1$ and $\Delta\Delta G_2$ have become more favorable than the paternal 3E5 IgG_3. Free energy loss is observed for the Fab 3E5 IgG_3 ($\Delta\Delta G > 0.5$ kcal/mol) with respect to the parental 3E5 IgG_3, with most of this loss coming from the encounter step ($\Delta\Delta G1$) (supplemental data, Fig. 2S). The binding energy differences for the transition states for the mAbs 3E5-P1 complexes revealed that the γ_1, γ_{2a}, and γ_{2b} C_H regions have more favorable activation energy for the transition state than that of γ_3 C_H domains, with the exception of Fab 3E5 IgG_3 where the binding energy ($\Delta\Delta G > 0.5$ kcal/mol) and the activation energy of the transition state ($\Delta\Delta G^{\ddagger} > 0.5$ kcal/mol) increased relative to the parental mAb (supplemental data, Fig. 3S).

The changes in the entropy of association (ΔS) (Fig. 4*D*) for the mAbs 3E5 to P1 follow a pattern similar to that of ΔG (Fig. 4*A*). We observed that for all mAbs 3E5 complexes, except Fab 3E5 IgG_{2a}, ΔS decreased at higher temperatures with Fab 3E5 IgG_{2a} being the highest. For all mAbs, except Fab 3E5 IgG_{2a}, a favorable ΔS was complemented by a favorable ΔH (supplemental data, Table 1S). For the Fab 3E5 IgG_{2a} an unfavorable ΔH was compensated by a favorable ΔS (supplemental data, Table 1S).

Molecular Modeling—In the absence of experimental structures, comparative protein structure modeling can be used to generate three-dimensional models for Abs and to put in a structural context the experimental observations and changes in biophysical properties. The three-dimensional structures of the Fab domains from the different 3E5 IgG subclasses have been modeled based on the x-ray structure of the highly homologous anti-GXM mAb 2H1 (Fig. 5*A*). At such a high level of sequence identity (>90%) comparative modeling can deliver a three-dimensional model with competitive accuracy to the resolution of a medium x-ray crystallographic solution (19).

Three regions of structural differences (identified as regions A, B, and C) were observed within the C_{H1} domain of 3E5 IgG isotypes (Figs. 5*B* and 6, *A–C*). Residues in these regions may form interchain and/or solvent electrostatic or hydrophobic interactions that differed between isotypes. Of particular importance are Asp^{180} and Thr^{183}, in regions A and B, respectively, because of their location at regions that have highly connected interactions. Furthermore, these two amino acids are not only important for their ability to form hydrogen bonds but also because they are located within an area of high electrostatic interactions between amino acids that could affect the structure of the Ag binding site (Fig.

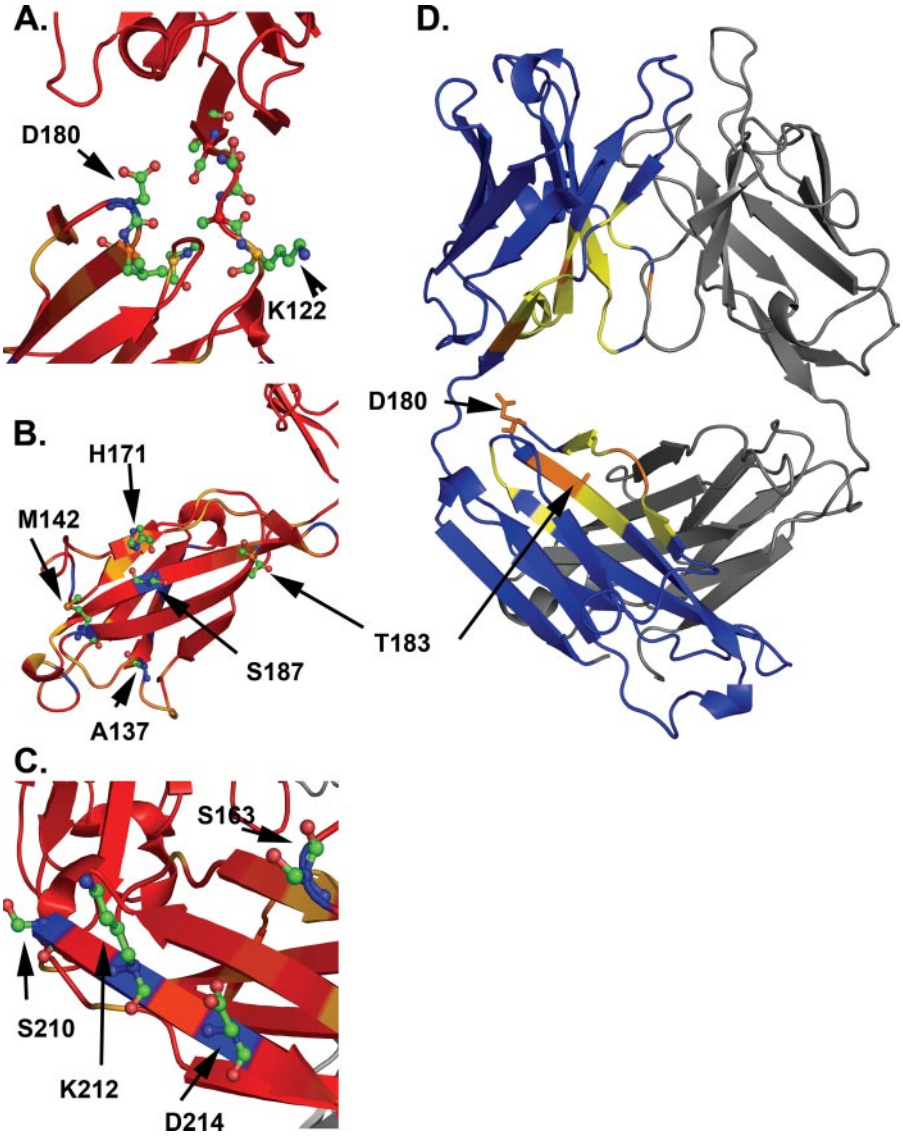

FIGURE 6. **Homology modeling analysis of mAb 3E5 C_{H1} domain.** Magnified views of regions A, B, and C are showed in *panels A*, *B*, and *C*, respectively. Side chains of amino acids with structural differences between C_{H1} domains of different IgG isotypes are indicated by *arrows*. *D*, amino acid connectivity analysis of mAb 3E5 IgG_1. Areas of high connectivity are indicted by *red* and *orange* (*red*, Zscore $>$ 2.0; *orange*, 1.5 $<$ Zscore $<$ 2.0). Medium connectivity residues are indicated in *yellow* (1.0 $<$ Zscores $<$ 1.5), and low connectivity is indicated in *blue* (Zscore $<$ 1.0). Light chain is shown in *gray*. Amino acids Asp^{180} and Thr^{183} are located in the *orange area* and are indicated by *arrows*. This figure was generated using PyMOL.

we tested the effect of pH and ethanol in the binding of the mAbs 3E5 to GXM. We examined the areas of greatest variability in the various C_H regions and hypothesized that changing the solvent and/or pH would perturb local interactions and result in differences in Ag binding for the various 3E5 IgG subclasses. These residues could possibly interact with water molecules or form hydrophobic or electrostatic interactions.

We used pH to perturb the charged interactions predicted by molecular modeling in the C_{H1} domain. We observed that mAbs 3E5 were able to bind to GXM at different pHs at room temperature. However, for 3E5 IgG_1 there was a decrease in binding relative to the other isotypes as the pH increased (Fig. 7, *A* and *B*). The pH changes may have a stronger influence in the electrostatic and hydrophobic interactions in the Ab combining site and/or its surroundings, thus resulting in pH-mediated conformational changes. This finding also correlates with the higher ΔG_1 for 3E5 IgG_1 with respect to the other isotypes, suggesting that this mAb forms more electrostatic and hydrophobic interactions at the binding site that could be easily disturbed by changes in pH. It is noteworthy that there was little or no difference between the binding curves of the four IgG subclasses at the pH used for Biacore analysis.

The binding of 3E5 IgG subclasses to GXM in ethanol (Fig. 7*C*) was different from that observed under buffer conditions (7). There was an increase in the relative binding affinity, where $IgG_{2b} > IgG_{2a} > IgG_3 > IgG_1$ to GXM (Fig. 7*C*). Ethanol changes the polarity and dielectric constant of the environment and decreases protein solubility. The change toward GXM binding was expected to come from changes caused by the removal of solvent molecules from the Ag binding site and its surroundings. This could cause polar groups that were exposed to become buried inside the protein consequently changing the IgG electrostatic and hydrophobic surface properties of IgGs. Since these mAbs have identical V regions, the contribution to these effects must originate from the differences of side chains in the C_H domains. These results correlate with the binding entropies, where 3E5 IgG_1 has the most favorable ΔS (Fig. 4*D*), likely because of changes in the hydrophobic interactions.

6*D*). It is notable that the SARIG calculations do not show the Ag binding site as a highly connected one. Hence, the few differences observed in the homology models of different mAbs in the C_{H1} domain, may have rather significant impact in the Ag binding site.

Ethanol and pH Affect Binding Patterns of mAb 3E5—Because molecular modeling predicted that there were no significant changes in conformation of the V region of these mAbs, we considered whether the observed residue changes in the C_H regions and the consequent perturbations in the solvent environment would translate into changes in affinity for Ag. The premise for these studies was to obtain supporting evidence for the concept that sequence differences in the C_{H1} domain of IgG isotypes could result in structural changes that propagated into the V region and altered binding properties. For that purpose

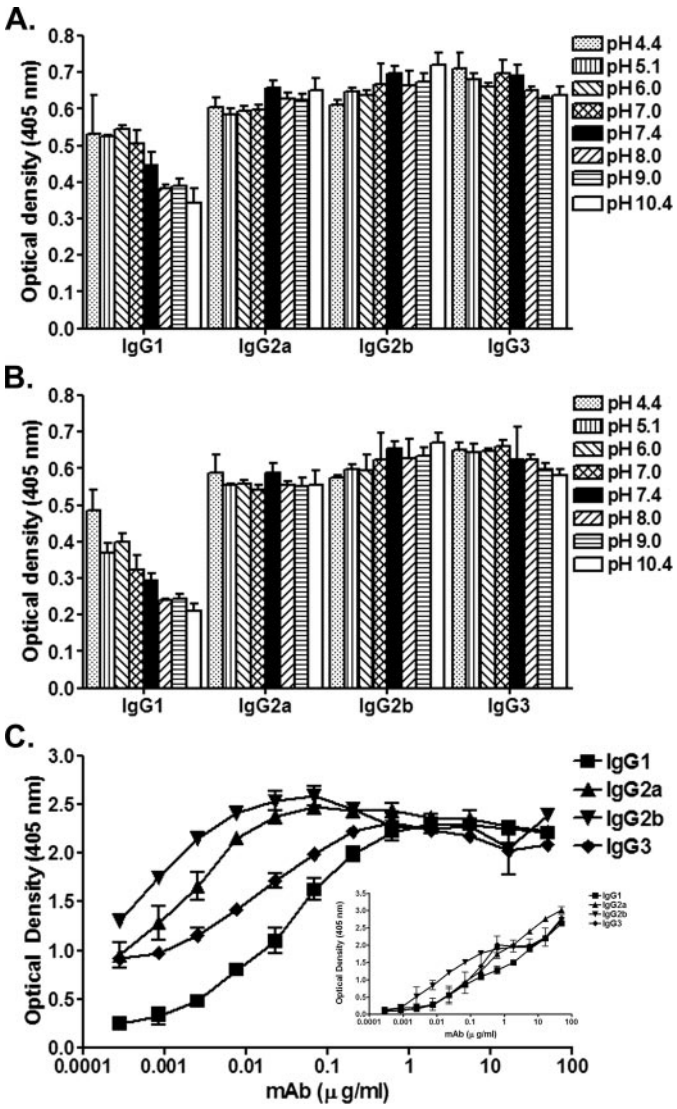

FIGURE 7. **Binding profiles of the mAbs 3E5 to GXM as a function of pH at two different concentrations by ELISA.** *Panels A* and *B* correspond to 0.6 and 1.9 μg/ml mAbs 3E5, respectively. Each *bar* represents a different pH of the binding buffer. *C*, binding profiles of the mAbs 3E5 in 5% ethanol to bound GXM on an ELISA plate. The *inset* shows the binding of 3E5 mAbs in TBS-1% BSA buffer conditions to bound GXM. Data represent the mean ± S.D. of three measurements.

mAbs 3E5 Exhibit Polyreactive Characteristics—The polyreactive properties of the 3E5 IgG switch variants were measured by a panel of antigens consisting of actin, tubulin, thyroglobulin, single-stranded DNA, and double-stranded DNA (Fig. 8). Polyreactivity was evident among these mAbs, showing differences in binding reactivity with the Ags used for the study. All mAbs show some degree of binding to thyroglobulin (Fig. 8*A*), whereas only IgG_3 shows binding reactivity for tubulin (Fig. 8*C*). In addition, the studied cross-reactants are not related to the capsular polysaccharide, GXM, thus showing that cross-reactivity does not only occur with closely related molecules.

DISCUSSION

For isotype-switched variant Abs with identical V regions to have different thermodynamic parameters in their interaction with a peptide, one must conclude that the molecular interactions between the peptide and the Ab paratope differ depending on the constant region. Different molecular interactions in turn imply different forms of complexes and thus differences in fine specificity. Consequently, mAbs with identical V regions differing in isotype can manifest variations in their fine specificity and functional affinity as a consequence of their associated C_H region.

The binding of mAbs 3E5 to a peptide mimetic of GXM are interactions of relatively low binding affinity, but the ability of the four IgG subclasses to discriminate among peptides indicates high specificity for these mAbs. Interestingly, these mAbs not only can bind to GXM-derived oligosaccharides and peptides that are mimetics of GXM with high specificity but they also bind to unrelated antigens, making this IgG set polyreactive or cross-reactive. Furthermore, the polyreactivity of a given V region is a function of its associated C_H region. Affinity was also influenced by C_H region, as Fab 3E5 IgG_3 had the lowest binding affinity within this set of mAbs. In contrast, Fab 3E5 IgG_{2a} had a higher affinity than the intact 3E5 IgG_{2a} or the parental 3E5 IgG_3. These observations suggest that structural differences in the C_{H1} domain are responsible for the differences in affinity constants and, consequently, for variations in Ag binding. The mechanism for this effect could involve transforming the structure of the binding site into a more kinetically competent form in mAbs with higher binding affinities (29). In this regard, it has been shown that segmental flexibility is controlled by the C_{H1} domain and the hinge regions of Abs (30, 31). However, binding differences due to the hinge do not explain the higher binding affinity obtained with Fab 3E5 IgG_{2a}. In the case of Fab 3E5 IgG_3, this molecule could be less flexible or have fewer interactions with the solvent, thus reducing the hydrophobic interactions and increasing the "hydrophobic effect," resulting in increased entropy.

The small structural variations predicted by the homology models of the Fab of mAbs 3E5 support our thesis that differences in fine specificity result from minor changes in the neighboring amino acid residues of the C_{H1} region. Consistent with this notion, homology modeling revealed that the Fab structures of mAbs 3E5 were very similar, and structural differences were expected to be below the level of x-ray crystallography resolution. This supports the use of a thermodynamic solution to approach differences in Ab-Ag complex formation as a function of isotype. The homology models identified three regions in the C_{H1} domain that potentially caused structural differences in the mAbs 3E5. The differences in C_{H1} domains could develop in structural isomers that could alter the association rates at which the Ab-Ag complex is formed. Thus, fine specificity differences might arise from even the minor variations in the side chains of the C_H domains, probably by structuring the Ab binding site into a more kinetically competent form. In addition, it is known that flexible side chains of polar and charged residues, such as Asp, Lys, Asn, Arg, and Ser, play an important role in binding (32). The homology models revealed that the three regions demonstrating structural differences involved at least one or more of these amino acids that could participate

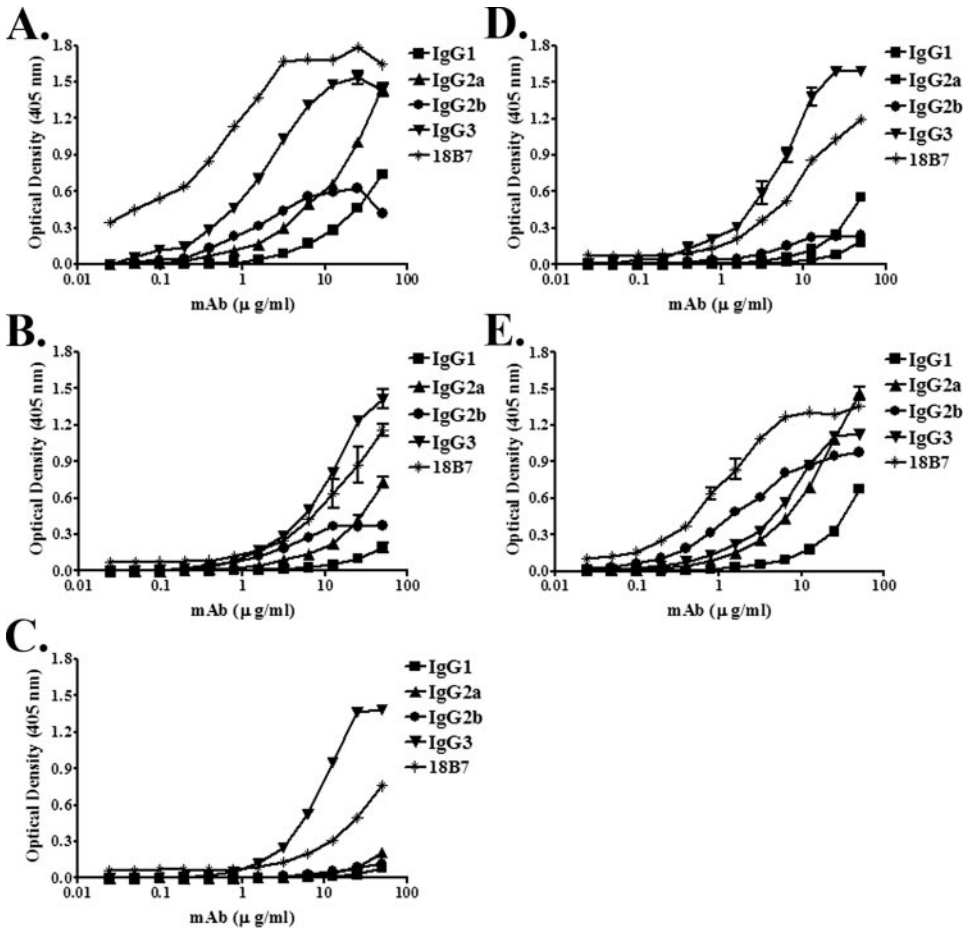

FIGURE 8. **Reactivity patterns of mAbs 3E5 against polyreactive antigens.** *Panels* corresponds to the binding profiles of 3E5 IgG switch variants to: *A*, thyroglobulin; *B*, double-stranded DNA; *C*, tubulin; *D*, actin; *E*, single-stranded DNA. Anti-GXM mAb 18B7 (IgG_1) was added as control. Data represent the mean ± S.D. of three measurements.

in the formation of electrostatic and hydrophobic interactions. Among the three regions, Asp^{180} and Thr^{183} in regions A and B, respectively, present in the C_{H1} domain of IgG_1 and IgG_{2a} isotypes, are of particular interest because of their ability to form hydrogen bonds. Furthermore, analysis of residues connectivity revealed that these amino acids are within a highly connected region. Highly connected areas were related to functionally important regions of proteins where a network of long range interactions between amino acids modulate direct or allosteric communications between proteins (22, 33, 34). Thus, the alterations in fine specificity and affinity observed for these mAbs could be a result of long range electrostatic interactions resulting from differences in the microenvironment of the C_H domains that affect the Ab combining site. Many studies support the idea that a limited number of V region differences (35–37) and non-contact residues can significantly change Ab conformation and function (36, 38). In addition, there is evidence that amino acid changes in the V_H region may induce different functional roles in the context of an altered H-chain microenvironment (36, 39) even if these residues are not within the binding site or do not directly necessary contribute to the total Ag binding (36, 39). Because these Abs share the same V region, changes in paratope conformation may well be attributed to changes in the microenvironment of the binding site due to the associated C_H.

Environmental variations such as in pH and ionic strength can lead to the redistribution of conformational states. Desolvation also plays a key role in determining the effect of electrostatics by counteracting the favorable electrostatics interactions formed between the Ag and Ab (40). The reactivity of mAbs 3E5 was not affected by small amounts of ethanol as a solvent. However, the affinity of binding in the alcoholic solutions increased relative to that observed in buffer without ethanol. This suggests that in the presence of ethanol more favorable hydrophobic interactions are formed between the Ab-Ag binding site and the solvent. Furthermore, by decreasing the pH, we observed a significant reduction in the binding of mAb 3E5 IgG_1 to GXM relative to the other isotypes. For this isotype, pH may have a greater influence on the alternation between a compact and a more open conformation, resulting in a "conformational switch" that affects Ag binding specificity. This also suggests that there are more interactions of polar and charged amino acids with the solvent occurring for 3E5 IgG_1 than for the other isotypes. Differences in the pH dependence of binding for the different isotypes raises the intriguing possibility of isotype-related differences in binding affinity and specificity for Ab-Ag complexes in acidic compartments such as phagosomes.

The ability of the immune system to produce Abs with different specificities through class switch recombination may be advantageous to the host in providing an additional source of diversity in the Ab response. Thus, the immune response could be enhanced by expressing a different isotype. This notion is supported by immunization studies with oxazolin, where upon antigen binding isotype-specific patterns arise, a feature observed only in autoimmune diseases (41). Amplification of the Ab immune response through isotype switching could conceivably allow for the formation of certain V region combinations that are self-reactive, which are not eliminated through the negative selection processes because of their low affinities. Thus, isotype switching could be a way to generate antibodies with wider specificity that still conserve their ability to bind to the original Ag and provide a way to manage the continuous genetic variation of pathogens, as well as facilitating the rapid recruitment of protective Abs against pathogens such as *Cryptococcus neoformans*, *Streptococcus pneumoniae*, and influenza virus.

The plasticity of the paratope site of an anti-carbohydrate Ab could allow for a convergence of specificities of Abs recognizing a common subset of antigenic determinants (9). Thus, rather than having to generate a new Ab with a different specificity, through a change of isotype combined with plasticity of the binding site, a "fit" to the Ag can be induced by isotype switching. This can be of particular importance for multivalent Ags, such as GXM, in which Abs with the same V region and different C_H region may recognize slightly different epitopes according to microenvironment variations induced by the associated C_H chain. This in turn would increase the heterogeneity of the Ab combining site and may be important for the development of Ab cross-reactivity and for Id networks; consequently, it could play a major role in immunoregulation of the humoral response. Reitan and Hannestad (42, 43) demonstrated that the anti-Id response can also be induced by monomeric IgM, IgA, and IgE molecules and even $F(ab')_2$ fragments, although the Fc regions of IgGs seem to have a dominant effect and induce long lasting unresponsiveness to the associated V regions. As idiotypic interactions dispense of antigens, they might operate in the selection of preimmune repertoires and therefore in the establishment of natural tolerance.

For the modeled structures, we assumed that the peptide-bound structures for the Fab of these mAbs were very similar, with only slight alterations in a few side chains. This supported the notion of Ab multispecificity due to the formation/change of hydrogen bonds or/and salt bridges rather than by hydrophobic interactions. Polyspecificity is also a characteristic observed in auto-Abs (44). Polyreactive antigen binding B cells, which can bind to and process endogenous host antigens from peripheral tissues and are found in the thymus, may contribute to immunological tolerance. If this turns out to be the case, then the B cell repertoire would have a dual function: high affinity Abs to protect against foreign invaders and low affinity polyreactive Ag-binding B cells to protect against autoimmune diseases by contributing to immunological tolerance. The recruitment of B cells expressing low affinity, polyreactive Abs may also reinforce self-tolerance in a constantly renewing of B lymphocytes (45).

Our study suggests another way of generating immune diversity. As such, the immunological memory could be affected to determine the course of the secondary response by the generation of Abs with identical V regions but different isotype, giving origin to higher or lower memory response depending on isotype. Given that isotype could affect specificity, Ag binding to the B cell receptor could directly trigger clonal expansion of isotype-restricted Ag-specific B cells. Consequently, the well known isotype restriction of anti-polysaccharide and anti-viral responses may reflect isotype-related effects on Ab specificity for an Ag.

Acknowledgments—We thank Dr. Liise-anne Pirofski for critical reading of the manuscript and Dr. Michael Brenowitz and Huiyong Cheng for assistance with SPR experiments.

REFERENCES

1. Ravetch, J. V., and Kinet, J. P. (1991) *Annu. Rev. Immunol.* **9,** 457–492
2. Tonegawa, S. (1983) *Nature* **302,** 575–581
3. Greenspan, N. S., Dacek, D. A., and Cooper, L. J. (1989) *Faseb. J.* **3,** 2203–2207
4. Cooper, L. J., Shikhman, A. R., Glass, D. D., Kangisser, D., Cunningham, M. W., and Greenspan, N. S. (1993) *J. Immunol.* **150,** 2231–2242
5. Morahan, G., Berek, C., and Miller, J. F. (1983) *Nature* **301,** 720–722
6. McCloskey, N., Turner, M. W., Steffner, P., Owens, R., and Goldblatt, D. (1996) *Immunology* **88,** 169–173
7. Torres, M., May, R., Scharff, M. D., and Casadevall, A. (2005) *J. Immunol.* **174,** 2132–2142
8. Janin, J. (1995) *Biochimie* (*Paris*) **77,** 497–505
9. Manivel, V., Bayiroglu, F., Siddiqui, Z., Salunke, D. M., and Rao, K. V. (2002) *J. Immunol.* **169,** 888–897
10. McLean, G. R., Torres, M., Elguezabal, N., Nakouzi, A., and Casadevall, A. (2002) *J. Immunol.* **169,** 1379–1386
11. Casadevall, A., Mukherjee, J., Devi, S. J., Schneerson, R., Robbins, J. B., and Scharff, M. D. (1992) *J. Infect. Dis.* **165,** 1086–1093
12. Spira, G., and Scharff, M. D. (1992) *J. Immunol. Methods* **148,** 121–129
13. Beck, A., Bussat, M. C., Zorn, N., Robillard, V., Klinguer-Hamour, C., Chenu, S., Goetsch, L., Corvaia, N., Van Dorsselaer, A., and Haeuw, J. F. (2005) *J. Chromatogr. B Analyt. Technol. Biomed. Life Sci.* **819,** 203–218
14. Benson, D. A., Karsch-Mizrachi, I., Lipman, D. J., Ostell, J., and Wheeler, D. L. (2006) *Nucleic Acids Res.* **34,** D16–D20
15. Berman, H. M., Westbrook, J., Feng, Z., Gilliland, G., Bhat, T. N., Weissig, H., Shindyalov, I. N., and Bourne, P. E. (2000) *Nucleic Acids Res.* **28,** 235–242
16. Altschul, S. F., Madden, T. L., Schaffer, A. A., Zhang, J., Zhang, Z., Miller, W., and Lipman, D. J. (1997) *Nucleic Acids Res.* **25,** 3389–3402
17. Rai, B. K., Madrid-Aliste, C. J., Fajardo, J. E., and Fiser, A. (2006) *Bioinformatics* (*Oxf.*) **22,** 2691–2692
18. Sali, A., and Blundell, T. L. (1993) *J. Mol. Biol.* **234,** 779–815
19. Fiser, A., and Sali, A. (2003) *Methods Enzymol.* **374,** 461–491
20. Sippl, M. J. (1993) *Proteins* **17,** 355–362
21. Laskowski, R. A., MacArthur, M. W., Moss, D. S., and Thornton, J. M. (1993) *J. Appl. Crystallogr.* **26,** 283–291
22. Amitai, G., Shemesh, A., Sitbon, E., Shklar, M., Netanely, D., Venger, I., and Pietrokovski, S. (2004) *J. Mol. Biol.* **344,** 1135–1146
23. Lipschultz, C. A., Li, Y., and Smith-Gill, S. (2000) *Methods* (*San Diego*) **20,** 310–318
24. Lipschultz, C. A., Yee, A., Mohan, S., Li, Y., and Smith-Gill, S. J. (2002) *J. Mol. Recognit.* **15,** 44–52
25. Selzer, T., and Schreiber, G. (1999) *J. Mol. Biol.* **287,** 409–419
26. Selzer, T., and Schreiber, G. (2001) *Proteins* **45,** 190–198
27. Davis, M. E., Madura, J. D., Sines, J., Luty, B. A., Allison, S. A., and McCammon, J. A. (1991) *Methods Enzymol.* **202,** 473–497
28. Kozack, R. E., d'Mello, M. J., and Subramaniam, S. (1995) *Biophys. J.* **68,** 807–814
29. Pritsch, O., Magnac, C., Dumas, G., Bouvet, J. P., Alzari, P., and Dighiero, G. (2000) *Eur. J. Immunol.* **30,** 3387–3395
30. Dangl, J. L., Wensel, T. G., Morrison, S. L., Stryer, L., Herzenberg, L. A., and Oi, V. T. (1988) *EMBO J.* **7,** 1989–1994
31. Schneider, W. P., Wensel, T. G., Stryer, L., and Oi, V. T. (1988) *Proc. Natl. Acad. Sci. U. S. A.* **85,** 2509–2513
32. Okamoto, A., Ishii, S., Hirotsu, K., and Kagamiyama, H. (1999) *Biochemistry* **38,** 1176–1184
33. Suel, G. M., Lockless, S. W., Wall, M. A., and Ranganathan, R. (2003) *Nat. Struct. Biol.* **10,** 59–69
34. Chennubhotla, C., and Bahar, I. (2006) *Mol. Syst. Biol.* **2,** 36
35. Hande, S., and Manser, T. (1997) *Mol. Immunol.* **34,** 1281–1290
36. Lavoie, T. B., Mohan, S., Lipschultz, C. A., Grivel, J. C., Li, Y., Mainhart, C. R., Kam-Morgan, L. N., Drohan, W. N., and Smith-Gill, S. J. (1999) *Mol. Immunol.* **36,** 1189–1205
37. Jeske, D. J., Jarvis, J., Milstein, C., and Capra, J. D. (1984) *J. Immunol.* **133,** 1090–1092

38. Foote, J., and Winter, G. (1992) *J. Mol. Biol.* **224,** 487–499
39. Greenspan, N. S., and Cooper, L. J. (1995) *Immunol. Today* **16,** 226–230
40. Chong, L. T., Duan, Y., Wang, L., Massova, I., and Kollman, P. A. (1999) *Proc. Natl. Acad. Sci. U. S. A.* **96,** 14330–14335
41. Luger, E., Lamers, M., Achatz-Straussberger, G., Geisberger, R., Infuhr, D., Breitenbach, M., Crameri, R., and Achatz, G. (2001) *Eur. J. Immunol.* **31,** 2319–2330
42. Reitan, S. K., and Hannestad, K. (2001) *Eur. J. Immunol.* **31,** 2143–2153
43. Reitan, S. K., and Hannestad, K. (2002) *Proc. Natl. Acad. Sci. U. S. A.* **99,** 7588–7593
44. Boffey, J., Nicholl, D., Wagner, E. R., Townson, K., Goodyear, C., Furukawa, K., Furukawa, K., Conner, J., and Willison, H. J. (2004) *J. Neuroimmunol.* **152,** 98–111
45. Varela, F. J., and Coutinho, A. (1991) *Immunol. Today* **12,** 159–166